CaB12H12: A promising salt for aprotic electrolytes in calcium-based secondary batteries

Andrea Ceppetelli, Carlos Castilla-Martinez, Eymerick Rousselot, Laure Monconduit, Umit Demirci, Sergio Brutti, Lorenzo Stievano

Journal of Energy Storage 108 (2025) 115012

Contents lists available at ScienceDirect

Journal of Energy Storage

journal homepage: www.elsevier.com/locate/est

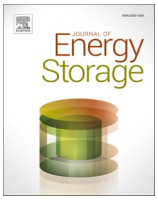

Research papers

$CaB_{12}H_{12}$: A promising salt for aprotic electrolytes in calcium-based secondary batteries

Andrea Ceppetelli [a,b], Carlos Castilla-Martinez [c], Eymerick Rousselot [b,c], Laure Monconduit [b,d], Umit B. Demirci [c], Sergio Brutti [a,e,f,*], Lorenzo Stievano [b,d,**]

[a] Department of Chemistry, University of Rome "La Sapienza", Rome, Italy
[b] Institut Charles Gerhardt Montpellier (ICGM), Univ. Montpellier, CNRS, ENSCM, Montpellier, France
[c] Institut Européen des Membranes (IEM), Univ Montpellier, CNRS, ENSCM, Montpellier, France
[d] Réseau sur le Stockage Electrochimique de l'Energie (RS2E), CNRS, Amiens, France
[e] Centro di Riferimento Nazionale per i Sistemi di Accumulo Elettrochimico di Energia (GISEL), INSTM, Florence, Italy
[f] Istituto dei Sistemi Complessi (ICS-CNR), CNR, Rome, Italy

ARTICLE INFO

Keywords:
$CaB_{12}H_{12}$
Dodecaborate
Electrolytes
Calcium batteries
Secondary batteries

ABSTRACT

Calcium dodecaborate, $CaB_{12}H_{12}$, is introduced and successfully tested as a promising salt for aprotic electrolytes in calcium-based batteries. The synthesis protocol for this innovative salt is both cost-effective and scalable, paving the way for environmentally safe and efficient manufacturing. The salt was incorporated into novel aprotic electrolyte formulations aimed at improving the reversibility of calcium plating and stripping, addressing a key challenge in calcium battery technology. Among the various tested formulations, a 0.25 M solution of $CaB_{12}H_{12}$ in *N*-methyl pyrrolidone exhibits superior performance, enabling reversible calcium plating/stripping at room temperature with overpotentials below 0.5 V at a current density of 0.1 $mAcm^{-2}$.

1. Introduction

The energy transition from a fossil fuel-based to a renewable, electricity-driven energy economy represents an extreme challenge, opening unprecedented technological questions in the field of energy storage. Scientists around the world are searching for innovative and competitive battery technologies for renewable energy integration in transportations, grid stability, and portable electronics [1]. The reversible electrochemical energy storage nowadays is dominated by the lithium-ion battery paradigm [1,2]. Nonetheless, this technology has limitations, related to the availability and costs of lithium commodities, as well as safety and manufacturing costs [3–5]. Since 2020, the European Union has classified lithium as one of the so-called "critical raw materials" due to its strategic relevance for its economy [6]. This scenario justifies the remarkable interests from public and private stakeholders in the so-called "beyond-lithium" batteries that may utilize also multivalent ion carriers derived from earth-abundant minerals such as Ca, Mg, Zn and Al [7].

In recent years, calcium batteries (CBs) have been emerging driven by the abundance of calcium and its promising electrochemical properties. Calcium is the 5th most abundant element on Earth's crust and the Ca^{2+}/Ca redox couple is characterised by the very low standard reduction potential of −2.87 V vs. SHE, much closer to Li (−3.04 V vs. SHE) than to Mg (−2.38 V vs. SHE), Al (−1.66 V vs. SHE) or Zn (−0.76 V vs SHE) [7,8]. Furthermore, Ca^{2+} transport kinetics in many crystalline solids are faster than those of Mg^{2+} and Al^{3+} ions thanks to the diffuse charge density [9,10]. However, the development of CBs is still at its early stage, with a key limitation being the lack of a clear evidence of reversible calcium metal plating/stripping at room temperature with overpotentials as low as those usually observed for lithium metal, using practical electrolyte formulations. This challenge derives from apparently unavoidable side reactions forming a stable and non-ionically conductive passivation film on the surface of the Ca metal anode, hindering reversible electrochemical activity [10–12]. Currently, the only electrolytes that allow the reversible plating/stripping of calcium metal with low overpotentials at room temperature require the use of Ca $(BH_4)_2$ as the electrolyte salt [13], which suffers from a limited electrochemical stability window preventing its use for the development of full cells.

Recently novel electrolytes based on the calcium tetrakis

* Corresponding author at: Department of Chemistry, University of Rome "La Sapienza", Rome, Italy.
** Correspondence to: L. Stievano, Institut Charles Gerhardt Montpellier (ICGM), Univ. Montpellier, CNRS, ENSCM, Montpellier, France.
E-mail addresses: sergio.brutti@uniroma1.it (S. Brutti), lorenzo.stievano@umontpellier.fr (L. Stievano).

https://doi.org/10.1016/j.est.2024.115012
Received 30 September 2024; Received in revised form 17 November 2024; Accepted 9 December 2024
Available online 19 December 2024

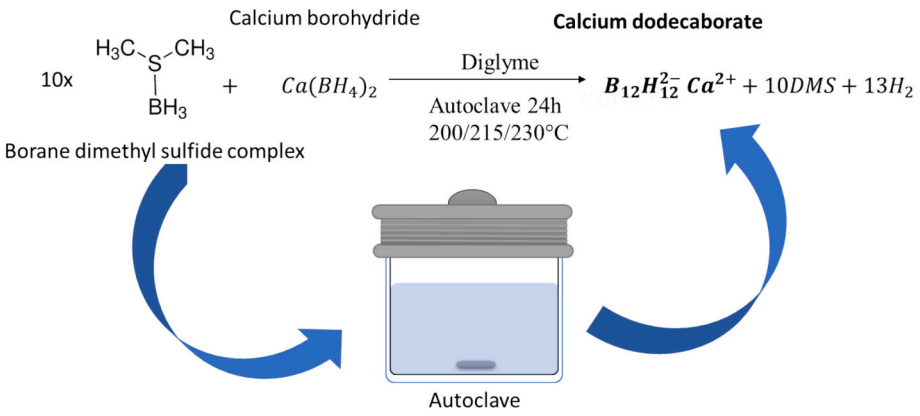

Fig. 1. Schematic representation of the synthesis of $CaB_{12}H_{12}$.

(hexafluoroisopropyloxy)borate salt ($Ca[B(hfip)_4]_2$) and its analogues have shown promise by enabling reversible Ca plating/stripping at room temperature together with a relatively large electrochemical stability window [14,15]. Nevertheless, the synthesis of these non-commercial salts releases large amounts of hydrogen gas [16] and requires a carefully controlled inert atmosphere (Ar with moisture level below 0.1 ppm) making large-scale manufacturing highly challenging. Kisu et al. also demonstrated that calcium monocarborane can be used as an efficient and stable electrolyte salt for CBs at room temperature [17]. Also in this case, however, the production of the salt is prohibitively expensive [18].

It is important to underline that the lack of readily available and cost effective calcium-based aprotic electrolytes has made the exploration and the experimental validation of new electrode materials for CBs very difficult. Owing to this, the development of efficient aprotic electrolytes is currently a critical prerequisite for the advancement of calcium-based energy storage systems.

In this study we introduce calcium dodecaborate, i.e., calcium dodecahydro-closo-dodecaborate ($CaB_{12}H_{12}$), for use in aprotic electrolytes for batteries. This salt was synthesized via a simple route inspired by the recent work of Wang et al. on alkaline dodecaborates (M $B_{12}H_{12}$; with M = Na, K) [19]. A schematic representation of the synthesis route of this innovative salt is shown in the Fig. 1.

Dodecaborate compounds are well known for their application in hydrogen storage [19,20] and to a lesser extent, as solid electrolyte in solid-state batteries [19,21,22]. Here it is demonstrated that liquid aprotic Ca^{2+} dodecaborate-based electrolytes based on non-conventional solvents such as *N*-methyl-2-pyrrolidone (NMP) enable the reversible plating/stripping of calcium metal.

2. Experimental section

2.1. Synthesis of calcium dodecahydro-closo-dodecaborate

The synthesis of $CaB_{12}H_{12}$ was carried out under inert atmosphere, either inside of an argon-filled glove-box (MBraun, $O_2 \leq 0.1$ ppm; $H_2O \leq 0.1$ ppm, $T = 25$ °C), or in a stainless-steel autoclave. We adapted the synthesis for $CaB_{12}H_{12}$ from the solvothermal method briefly schematised in Fig. 1 and previously reported elsewhere [19]. In a typical experiment, 0.04 g of $Ca(BH_4)_2$ was dissolved in 12 mL of anhydrous dimethoxyethane (DME) under stirring for 15 min. The solution was transferred to a Teflon liner and then, 1.2 mL of borane dimethylsulfide ($DMS{\cdot}BH_3$) was added to the system. The Teflon liner was then placed in an autoclave, which was sealed before being transferred outside the glove-box and placed in an oven at room temperature. The temperature was increased by 20 °C every 10 min up to the required temperature. The autoclave was held at this temperature for 24 h, then cooled to room temperature. Three synthesis temperatures were investigated: 200°, 215° and 230 °C. After cooling, the autoclave was returned to the glove-box; the recovered solid was filtered and washed with fresh DME (3 × 10 mL), and finally dried overnight under vacuum. From this point on, samples will be labelled $CaB_{12}H_{12}$@T (T = 200°, 215° or 230 °C), depending on their respective autoclave reaction temperature.

Table 1
Schematic representation of the electrolyte formulations.

Salt	Conc. (M)	Solvent	Solubility
$CaB_{12}H_{12}$@200 °C	0.25	DMSO	Partial (opalescent)
$CaB_{12}H_{12}$@215 °C	0.1–0.25-0.5	NMP	Partial (opalescent)
	0.25	ACN	No (colloidal precipitate)
	0.25	DMSO	Partial (opalescent)
$CaB_{12}H_{12}$@230 °C	0.25–0.5	DMSO	Partial (opalescent)
	0.1	NMP	Yes
	0.25–0.5	NMP	Partial (opalescent)
	0.25	DME/THF 1:1 (v/v)	No (colloidal precipitate)

2.2. Physico-chemical characterization

The synthesized samples were characterised by infrared spectroscopy (IR) using a Nexus spectrometer (ThermoFisher, equipped with an attenuated total reflection accessory from 600 to 4000 cm^{-1}). The samples were transferred to the IR apparatus in a vial under Ar atmosphere to minimize the direct contact with ambient air. Complementary nuclear magnetic resonance (NMR) analyses were carried out with a BRUNKER Ultrashield Avance 400 (^{11}B nucleus, 128 MHz, deuterated solvent: dimethyl sulfoxide DMSO).

2.3. Electrolyte formulation and preparation

The electrolyte formulations obtained by using the three synthesized $CaB_{12}H_{12}$@200/215/230 salts are summarized in the Table 1. All solvents (i.e., DME, dimethylsulfoxide (DMSO), tetrahydrofuran (THF), acetonitrile (ACN), and NMP) used for the electrolyte formulation (anhydrous grade from Sigma Aldrich/Merck) were opened and dried for 5 days with activated molecular sieves (3A, Sigma Aldrich/Merck) in the glove-box, before use. Commercial 1 M $LiPF_6$ solution in ethylene carbonate/dimethyl carbonate 1:1 vol mixture (LP30, Solvionic) was used for calibration purposes in the conductivity tests. Electrolytes were prepared by adding a weighted amount of $CaB_{12}H_{12}$ to the selected solvent in the glove-box followed by a 1 week stirring in sealed vials also kept inside the same glove-box. One additional electrolyte was formulated starting from the 0.5 M solution of $CaB_{12}H_{12}$@215 in NMP modified by the addition of 0.02 M boron trifluoride diethyl etherate

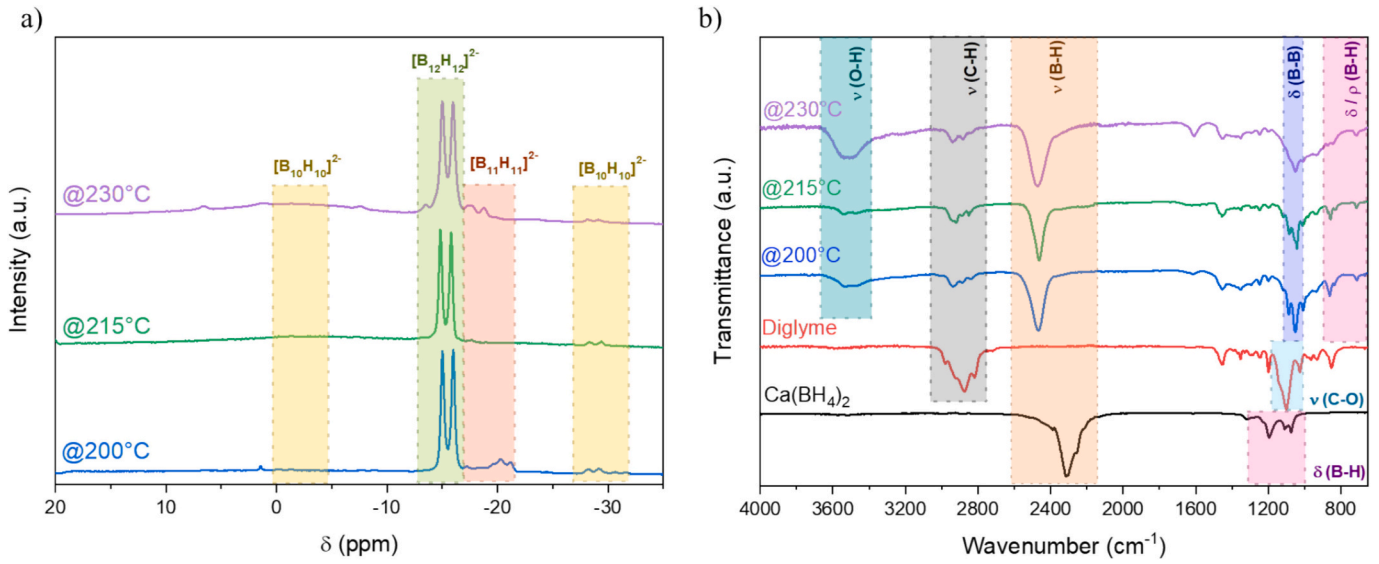

Fig. 2. (a) ^{1}H coupled ^{11}B NMR spectra of the solids obtained after synthesis at 200, 215 and 230 °C (the solids were dissolved in DMSO-d_6); (b) IR spectra of Ca$(BH_4)_2$, DME and of the $CaB_{12}H_{12}$ synthesized salts at three different temperatures.

(BF_3OEt_2, Sigma Aldrich) as an additive. All materials handling was performed inside an argon-filled glove-box.

2.4. Electrochemical tests

Calcium metal disk electrodes with a diameter of 9 mm were punched out from a Ca metal foil (ACI alloy Inc.). The surface of the calcium metal disks was scratched with a scalpel immediately before use. Whatman glass fibre separators (GF/A Cytiva, thickness 0.26 mm) were soaked with a known volume (80 μL) of each electrolyte during cell assembly (ECC-STD laboratory cells by El-Cell Gmbh) inside an Ar-filled glove-box. Symmetric Ca | electrolyte | Ca cell configurations were employed for preliminary electrochemical experiments using linear sweep voltammetry (LSV) and cyclic voltammetry (CV) at scan rates of 10 and 2 mV s^{-1}, respectively, as well as for advanced tests by galvanostatic cycling (GC) and electrochemical impedance spectroscopy (EIS) in the frequency range of 1 M – 100 m Hz at an amplitude of 5 mV. Stainless steel (SS) electrodes were employed as blocking electrodes in a symmetric configuration: SS | electrolyte | SS, for conductivity tests performed by EIS. Additionally, the asymmetric SS | electrolyte | Ca configuration was employed to evaluate the electrochemical stability window (ESW) of the electrolyte by LSV and CV.

In order to verify the successful deposition of Ca metal onto an inert substrate, a specific asymmetric cell (Ca | electrolyte | Au) was subjected to extended galvanostatic plating, and the nature and morphology of the deposited material was characterised by scanning electron microscopy (SEM) coupled with energy dispersive X-ray (EDX) analysis (Oxford Instruments X-Max 50 mm2), as well as by optical microscopy (Keyence VHX-7100). All electrochemical tests were carried out using Biologic MPG and VSP electrochemical testing devices.

3. Results and discussion

3.1. Nuclear magnetic resonance

The ^{11}B NMR spectra of the solid calcium salts obtained at 200, 215 and 230 °C (Fig. 2a) show an intense doublet centred at −15 ppm, assigned to the 12 boron atoms of the $[B_{12}H_{12}]^{2-}$ anion [20,23–25]. The predominance of this signal is a qualitative indication of the successful synthesis of $CaB_{12}H_{12}$. Two additional doublets centred at −29 ppm and −1 ppm are also observed in the spectra, indicating the formation of the $[B_{10}H_{10}]^{2-}$ anion [26]. $CaB_{12}H_{12}$@200 °C and $CaB_{12}H_{12}$@230 °C also show one supplementary multiplet between −16 and −22 ppm, which is attributed to traces of the $[B_{11}H_{11}]^{2-}$ anion [22].

Overall, the syntheses produced samples constituted by a large majority of calcium dodecaborate and minor amounts of Ca decabonare and Ca undecaborane. Having the weakest signals at −29, −1 and between −16 and −22 ppm, the samples synthesized at 215 °C are the purest. It is to be noted that the lack of signals between 5 and 20 ppm allows discarding the presence of species containing B—O bonds such as borates, confirming that the O—H bonds observed in the IR spectra are due to the adsorbed water (vide infra).

3.2. Infrared spectroscopy

The IR spectra of the samples synthesized at different temperatures are shown in Fig. 2b together with those of commercial Ca$(BH_4)_2$ and DME, measured as references. The spectrum of commercial DME shows the C—H stretching and bending bands in the ranges 2700–3000 and 1200–1400 cm^{-1}, respectively. The intense peak centred at 1050 cm^{-1} corresponds to the C—O stretching mode of the molecule. The Ca$(BH_4)_2$ spectrum shows bands between 2200 and 2400 cm^{-1} corresponding to the B—H stretching modes, and an additional group of signals between 1000 and 1300 cm^{-1} attributed to the deformation and bending modes of the BH_4^- anion [27,28].

The spectra of the $CaB_{12}H_{12}$ samples synthesized at different temperatures are very similar: the B—H stretching mode consistently appears in the 2350–2600 cm^{-1} region, similar to other dodecahydro-*closo*-dodecaborates, with a slight shift compared to Ca$(BH_4)_2$ [29,30]. Remarkably, the B—H stretching bands of Ca$(BH_4)_2$ are absent in all synthesized $CaB_{12}H_{12}$ samples, indicating a complete transformation of the borohydride precursor. The peak centred at 1050 cm^{-1} corresponds to the stretching mode of the B—B bonds in the boron cage, while the bands between 650 and 800 cm^{-1} correspond to the B—H rocking and bending modes [26,31]. The broad band between 3300 and 3600 cm^{-1} is assigned to the O—H stretching vibrations, likely indicating adsorbed water molecules (vide supra, Section 3.1). All synthesized samples also show bands between 2700 and 3000 cm^{-1}, which are attributed to C—H stretching modes, most probably due to traces of diglyme in the final product.

3.3. Electrolyte formulations and potentiodynamic survey

A summary of the prepared electrolyte formulations is presented in

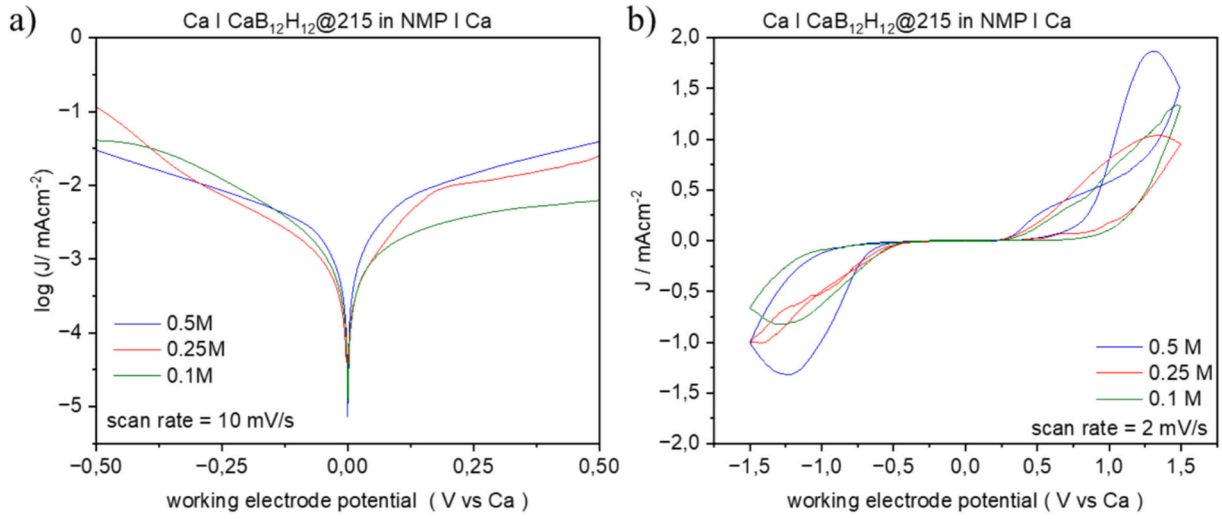

Fig. 3. a) LSV and b) CV of 0.1, 0.25 and 0.5 M $CaB_{12}H_{12}$@215/NMP electrolytes.

Table 1.

Calcium dodecaborate shows a limited solubility in all the tested solvents: DMSO, NMP, ACN and DME/THF. Dissolution in ACN and DME/THF leads to a viscous colloid, whereas solutions in DMSO and NMP form an opalescent precipitate, very stable upon time, with the only exception of the clear 0.1 M solution in NMP of $CaB_{12}H_{12}$ synthesized at 230 °C. Notably, this is the lowest salt concentration among those tested. Apparently, no precipitation or phase segregation was observed in DMSO and NMP solutions containing the opalescent precipitate. A possible explanation could be the different solubilities of dodeca-, undeca- and decaborane either in NMP or DMSO. In fact, the clearest solutions are observed for the $CaB_{12}H_{12}$@230 salt that contains undecaborane impurities but is likely free of decaborane. On the contrary, both $CaB_{12}H_{12}$@215 and $CaB_{12}H_{12}$@200, that are free of undecaborane but contain decaborane impurities, lead to opalescent suspensions. As a result, a filtration step was attempted; however, we observed that this process reduced the salt's electrochemical activity, with more pronounced deactivation in subsequent cycles compared to the unfiltered electrolyte (Fig. S2). This observation suggests a beneficial role of the insoluble particles. Therefore, further research was conducted without filtering the electrolyte.

A full survey of the electrochemical activity in LSV and CV tests of all $CaB_{12}H_{12}$-based electrolytes is shown in the supplementary information (SI, Fig. S1a and b, respectively). Our systematic analysis suggests that $CaB_{12}H_{12}$@215 and $CaB_{12}H_{12}$@230 in NMP electrolytes outperform the other formulations in terms of plating/stripping efficiency, reversibility and kinetics. Based on these preliminary results, further analysis of the electrochemical activity of both electrolytes based on $CaB_{12}H_{12}$@215 and $CaB_{12}H_{12}$@230 in NMP was carried out, comparing the impact of the calcium dodecaborate concentration, namely 0.1, 0.25 and 0.5 M, on the electrochemical activity (see SI, fig. S3). As expected, the electrolytes formulated with the highest salt concentration (0.5 M) exhibited the most intense peak currents in CV. However, $CaB_{12}H_{12}$@230-based electrolytes show a more rapid deactivation compared to $CaB_{12}H_{12}$@215-based formulations for all the three salt concentrations. Such a faster deactivation rate for the $CaB_{12}H_{12}$@230 solutions might be due the higher content in calcium undecaborane in this salt. Based on the results of this systematic preliminary survey, the following section focuses on the characterization of the $CaB_{12}H_{12}$@215 in NMP electrolytes.

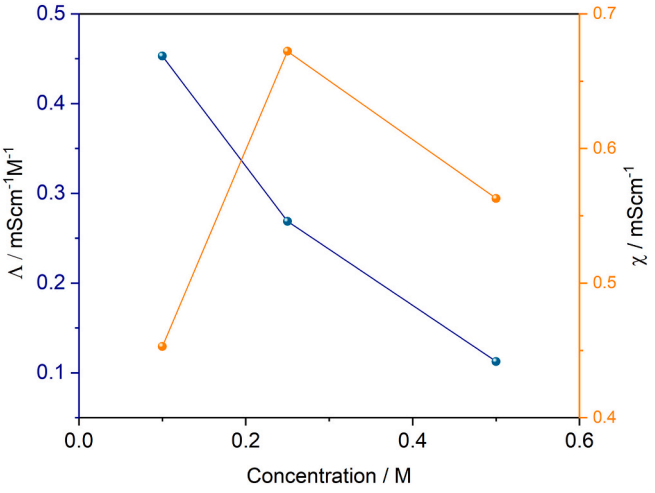

Fig. 4. Conductivity of the 0.1, 0.25 and 0.5 M $CaB_{12}H_{12}$@215/NMP electrolytes measured at room temperature.

3.4. *Electrochemical characterization of the $CaB_{12}H_{12}$@215 in NMP electrolytes*

The LSV curve and the firsts CV cycles for the $CaB_{12}H_{12}$@215 in NMP electrolyte at the three concentrations are shown in the Fig. 3a-b.

The LSV curves were fitted by using the simplified Buttler-Volmer equation (cf. Eq. (E1)) to evaluate quantitatively the fundamental kinetic parameters of the reversible Ca redox reaction in this solvent.

$$J = J^{o} \bullet \left(e^{(E-E^{o})/\beta_a} - e^{(E-E^{o})/\beta_c}\right) \quad \text{(E1)}$$

In this equation, J and J° are the measured current density and the exchange current density, respectively, E and E° are the measured cell voltage and the thermodynamic redox potential of the $Ca^{2+}(solv) + e^{-} \rightarrow Ca(s)$ reduction process, while β_a and β_c are the so-called anodic and cathodic Tafel coefficients. The Buttler-Volmer fitting results of the datasets in Fig. 3a are summarized in the Table 2.

Surprisingly, despite the monotonic changes of both Tafel coefficients with the increasing salt concentration, the exchange current density shows an inverted volcano trend, being very similar for 0.5 and 0.1 M and three times smaller for the 0.25 M formulation. At the same time, the redox reaction shifts from anodic to cathodic limitation, showing a symmetric behaviour only in the 0.25 M formulation, with

Table 2
Result of the Buttler-Volmer fitting for $CaB_{12}H_{12}$@215 for the three concentrations.

$CaB_{12}H_{12}$@215	0.1 M	0.25 M	0.5 M
$J^{\circ}\,(\mu A/cm^2)$	2.32	0.85	2.24
β_c	0.27	0.56	0.65
β_a	0.73	0.44	0.35

similar β-values.

To shed further light on this peculiar electrokinetic behaviour, electrolyte conductivities were measured for all three concentrations by EIS at room temperature. By using the LP30 solution as a calibration standard [32], the electrolyte total (χ) and molar (Λ) conductivities were determined. The results are shown in Fig. 4 and summarized in Table S6.

In all cases, the total conductivities are below 1 mS cm^{-1}, well below the LP30 benchmark and in line with the recent literature concerning calcium salts in aprotic electrolytes [33]. These results suggest a much stronger solvation of Ca^{2+} in NMP compared to Li^{+} in organic carbonates. Remarkably, the conductivities show non monotonic trend similar to a volcano shape, reaching a maximum value for the 0.25 M formulation. On the other hand, the molar conductivities show a monotonic decreasing trend with the salt concentration, following the expected empirical trend linearized by the Kohlrausch's law (i.e., $Ln(\Lambda)$ *vs.* $\sqrt{c}$, where c is the nominal molarity of ions) with a correlation coefficient $R^2 = 0.99$ and an estimated limiting molar conductivity at infinite dilution of 1.5 ± 0.5 mS cm^{-1}.

The volcano trend of the total conductivities matches the reversed-volcano shape of the Tafel parameters summarized in Table 2 for the same formulations, indicating that the calcium plating/stripping kinetics in $CaB_{12}H_{12}$/NMP electrolytes are not diffusion controlled. In fact, the smallest J° is observed in the 0.25 M formulation, which has the highest total conductivity at room temperature. This suggests that the reorganization energy of the electrolyte at the electrode surface plays a relevant role in enhancing or limiting the electron transfer. In fact, the measured values of total conductivity indicate a strong solvation of Ca^{2+} ions in NMP, unavoidably implying a positive desolvation enthalpy change. It has to be taken into consideration that this result could also imply a very weak dissociation and solvation of the salt in NMP. While further interpretations of these data would be too speculative, additional fundamental work is needed to decouple the various competitive effects that drive the kinetics of electrochemical calcium metal plating/stripping in aprotic media. However, this goes beyond the scope of this work.

The ESW of the three $CaB_{12}H_{12}$@215/NMP electrolytes was evaluated by CV in asymmetric cells Ca | $CaB_{12}H_{12}$@215 in NMP | SS with salt

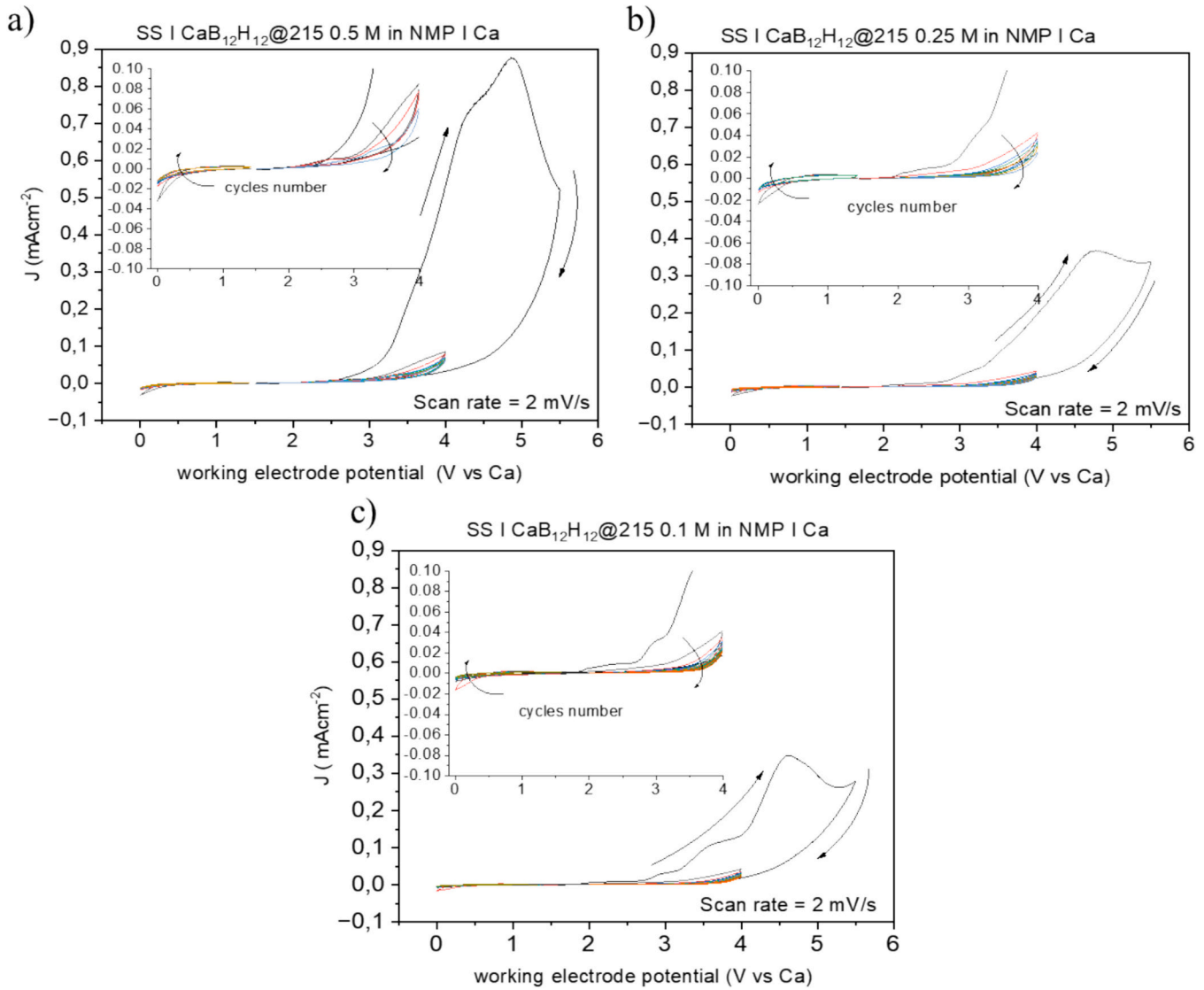

Fig. 5. Electrochemical stability window of (a) 0.5 M, (b) 0.25 M and (c) 0.1 M $CaB_{12}H_{12}$/NMP electrolytes.

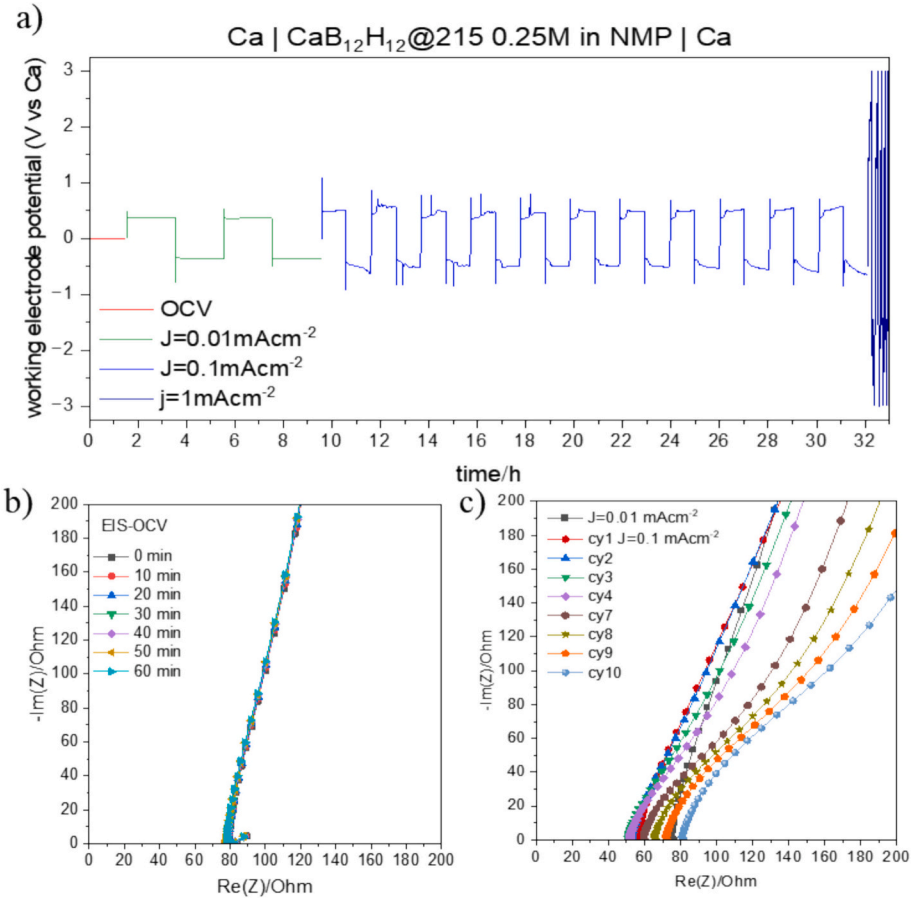

Fig. 6. Galvanostatic/EIS signatures of a Ca | 0.25 M $CaB_{12}H_{12}$@215/NMP | Ca cell: (a) evolution of the working electrode potential during the GC test; (b) EIS performed before cycling at OCV and (c) EIS performed upon cycling after each discharge step.

concentrations of 0.1, 0.25 and 0.5 M. The results of these measurements are shown in the Fig. 5.

The ESW of the studied electrolytes exhibits almost negligible cathodic degradation down to 0 V vs. Ca^{2+}/Ca and an anodic stability up to 2.7 V with current below 20 μA on the first cycle and 3 V vs. Ca^{2+}/Ca after the first oxidation cycle. Indeed, degradation current densities below 20 μA/cm^2 are observed at 3 V vs. Ca^{2+}/Ca for the three formulations, from the second cycle onwards. This result suggests the formation of a stable cathode electrolyte interphase (CEI) over the surface of the SS electrode during the first electrochemical cycle. As expected, the 0.25 M electrolyte exhibits reduced degradation currents compared to the 0.5 M concentration, indicating that the degradation is mainly due to the decomposition of the salt anion. When comparing the two lower concentrations, the 0.1 M electrolyte shows a slightly smaller anodic area than that of the 0.25 M solution, revealing also distinct reaction steps: a first one around 3.5 V and a second at 4.5 V vs Ca^{2+}/Ca. The initial step, up to approximately 3.5 V, is similar to that of the 0.25 M solution, and is likely caused by the initial degradation of the solvent. The following degradation step involves the salt and the formation of the CEI, with occurs to a lesser extent in the more diluted solution. This hypothesis is supported by the results shown in Fig. S4, where the anodic portions of the CV of the three formulations are overlaid to that of pure NMP. In addition, comparable oxidative stability around 3 V vs. Na^+/Na are observed in $Na_4(B_{12}H_{12})$ ($B_{10}H_{10}$) and $Na_4(CB_{11}H_{12})_2(B_{12}H_{12})$ and a similar behaviour is observed in yLi ($B_{10}H_{10-y}$), where a small irreversible oxidative current is seen around 2.8 V vs. Li^+/Li, which is not present in subsequent cycles [34].

In order to observe the effective formation of calcium metal during plating with the 0.5 M $CaB_{12}H_{12}$@215/NMP electrolyte, a long chronopotentiometric deposition of calcium was performed on a gold substrate at a current density of 0.01 mA cm^{-2}. Post mortem optical light microscopy and EDX analysis (cf. Fig. S5) of the electrode recovered from this cell confirm the successful deposition of Ca metal particles on the gold surface.

Once the ESW for both electrolyte formulations was determined and the effective plating of calcium metal was experimentally proven, the galvanostatic performance of Ca | electrolyte | Ca symmetric cells was measured. The results are shown in Figs. 6 and 7 for the 0.25 M and 0.5 M electrolytes, respectively. EIS measurements were carried out before GC to evaluate the spontaneous chemical reactivity of the electrolytes towards the calcium metal electrodes, as well as after each discharge step to monitor the evolution of the working electrode/electrolyte interface.

Overall, both electrolyte formulations support reversible galvanostatic plating/stripping cycles at applied currents up to 0.1 mA cm^{-1}, with overpotentials below 1 V, as shown in the Figs. 6a and 7a. Both electrolytes show stable and constant working potentials at 0.01 $mAcm^{-2}$ with symmetric overpotentials below 0.5 V. The 0.25 M electrolyte maintain this excellent performance also at 0.1 $mAcm^{-2}$ whereas the 0.5 M solution becomes unstable and its overpotential eventually increases, producing a voltage hysteresis between discharge and charge of ~2.5 V. This last value is about 60 % higher than the performance of the 0.25 M electrolyte. At current densities of 1 mA cm^{-2}, however, neither electrolyte is able to sustain reversible calcium metal plating/stripping. It is worth noting that at current densities higher than 0.01 mA cm^{-2}, voltage spikes appear in the GC voltage profiles. This feature is a direct indication of abrupt changes in the electrochemical active surface of the calcium metal electrodes, and can be attributed to several

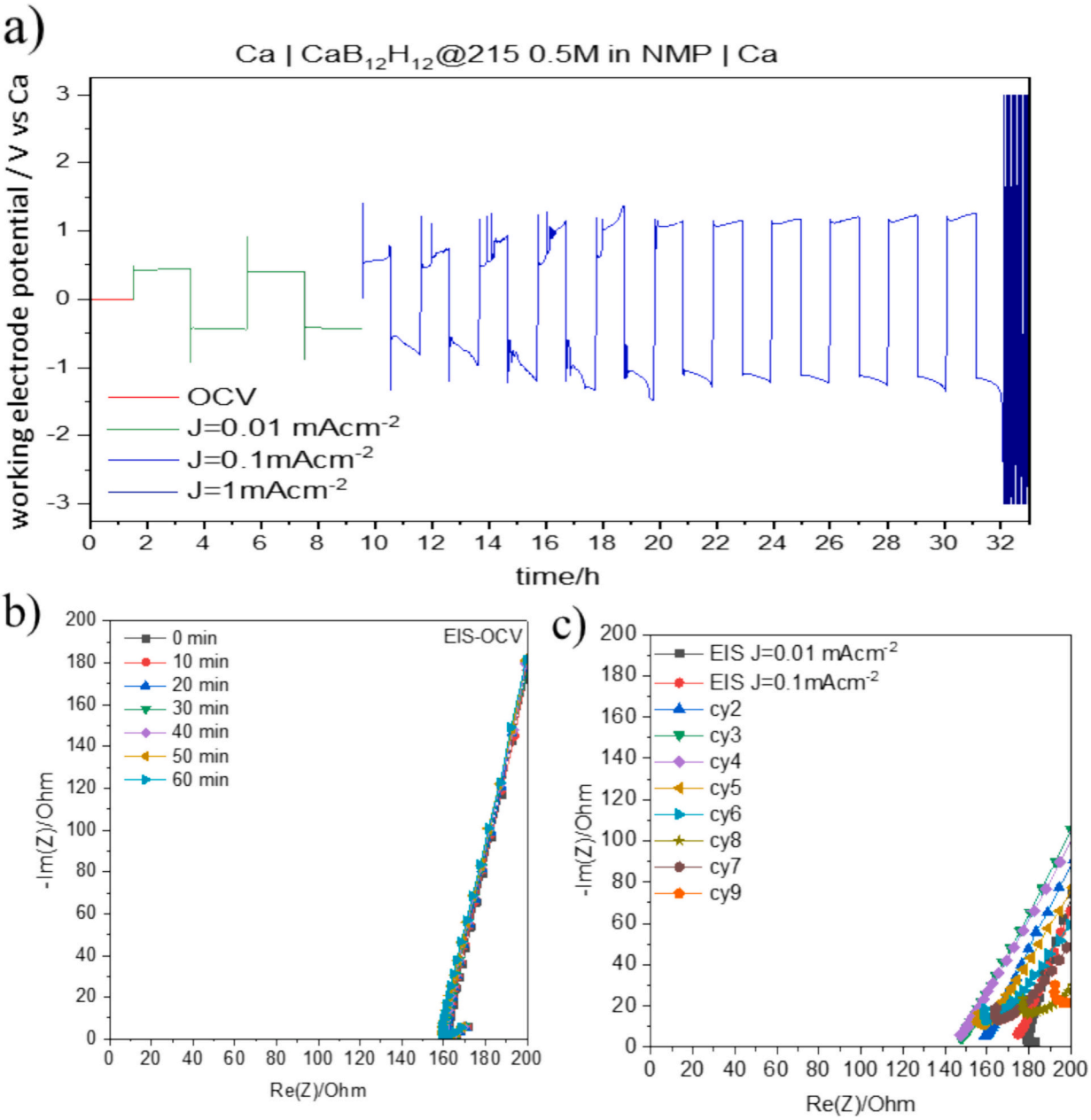

Fig. 7. Combined galvanostatic/impedance test results: Ca | 0.5 M $CaB_{12}H_{12}$@215/NMP | Ca cell: (a) evolution of the working electrode potential during the GC test; (b) EIS performed before cycling at OCV and (c) EIS performed upon cycling after each discharge step.

factors, including the formation of microdendrites, the breakdown of the SEI and gas release originating from parasitic chemistries [35–38].

Focusing on the impedance response of the working electrode/electrolyte interfaces, limited parasitic reactivity is observed upon cycling for both electrolytes (Figs. 6b-c and 7b-c). Before cycling, the impedance response remains stable over time in the high frequency range. In particular, both electrolyte formulations exhibit an almost constant high frequency Z_{real} value during the preliminary OCV test before GC, confirming a negligible spontaneous consumption of Ca^{2+} ions for the formation of the so-called natural solid electrolyte interphase (SEI) [39]. Moreover, the overall impedance spectra from high to low frequencies show a very large semi-circular feature with a diameter of tenths of kΩ for both 0.25 and 0.5 M formulations, with maxima in the 1–0.1 Hz range (cf. Fig. S8). As a consequence, the time constant of this active interface is in the seconds range, in agreement with the occurrence of the charge transfer process involved in Ca-plating/stripping.

Upon cycling, the EIS response of both electrolytes grows gradually cycle by cycle in the high-frequency range, with the Z_{real} intercept taking values 1.6 and 1.7 times higher than the initial ones for the 0.25 and the 0.5 M electrolytes, respectively. This trend suggests the irreversible consumption of electrolyte Ca^{2+} ions in parasite reactions, leading to a gradual decrease of the electrolyte conductivity. These degradation reactions most probably involve the formation of insoluble Ca-containing by-products at the surface of the working electrode. Similarly, the relative increase in the high-frequency Z_{real} intercept suggests that these parasitic reactions are not concentration-dependent but are likely driven by the inadequate dielectric properties of the SEI layer, unable to prevent the charge transfer from the electrode to the electrolyte solvent molecules.

Summarising, the aprotic electrolyte based on $CaB_{12}H_{12}$ in NMP enables reversible calcium metal plating/stripping on calcium electrodes, at room temperature. Apparently the 0.25 M formulation slightly

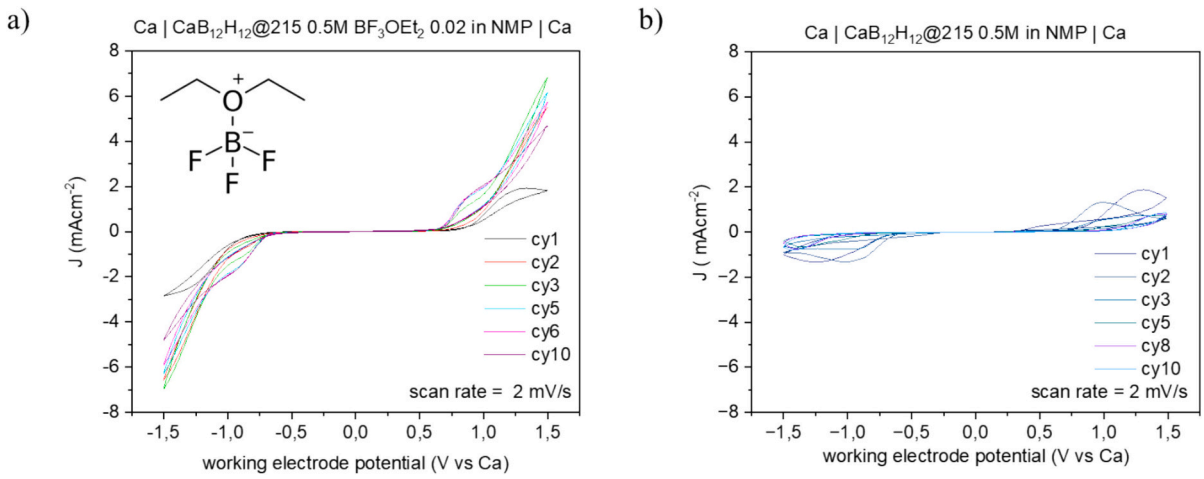

Fig. 8. CV of the (a) 0.5 M $CaB_{12}H_{12}$@215/NMP electrolyte containing 0.02 M BF_3OEt_2 and (b) pristine 0.5 M $CaB_{12}H_{12}$@215/NMP electrolyte.

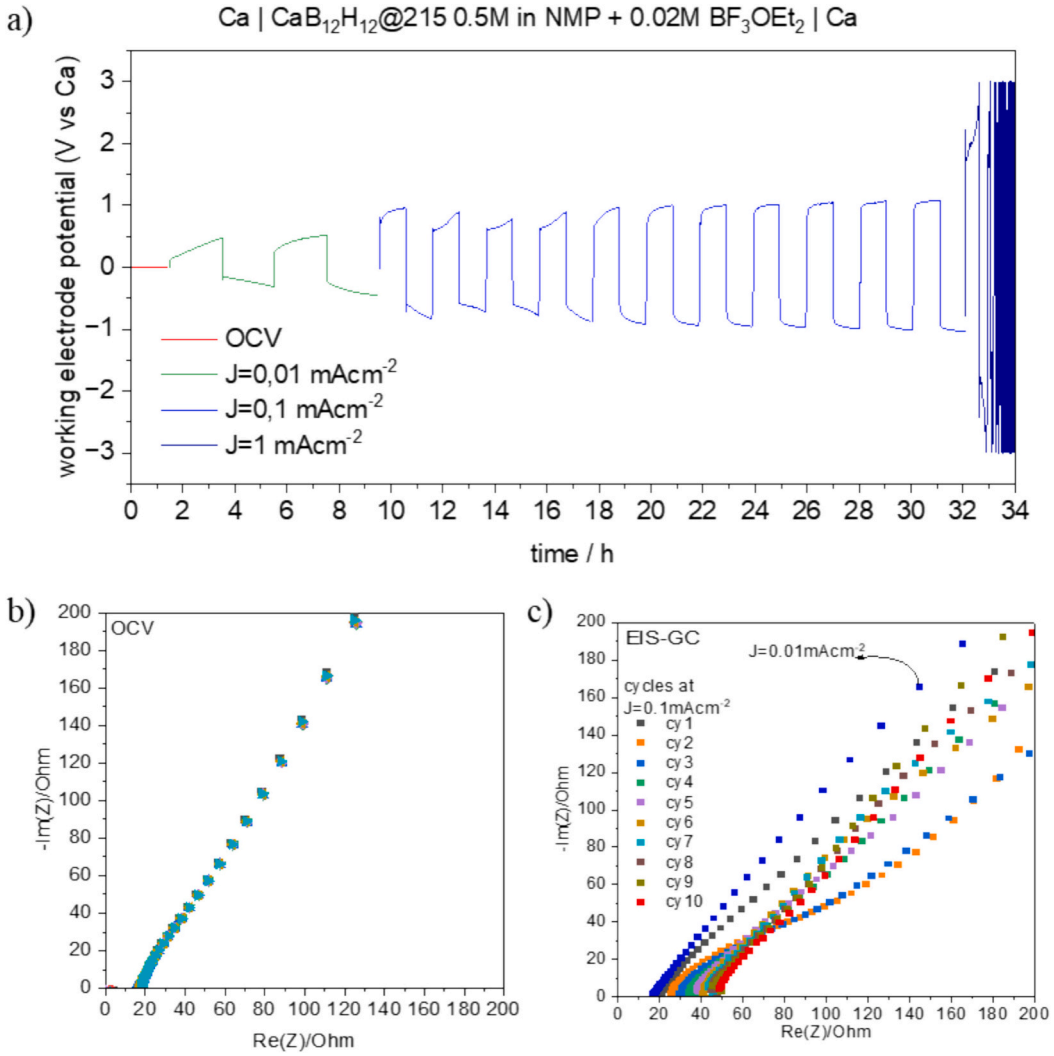

Fig. 9. GC/EIS test of a Ca | 0.5 M $CaB_{12}H_{12}$@215/NMP + 0.02 M BF_3OEt_2 | Ca cell: (a) evolution of the working electrode potential during GC; (b) EIS signal measured at OCV and (c) evolution of the EIS signal during cycling.

outperforms the 0.5 M one, likely thanks to a better balance between conductivity and Buttler-Volmer electrode kinetics during the plating/stripping process. In both cases, however, the electrolyte/electrode interphase on calcium metal is electrochemically unstable, leading to an inefficient SEI layer that cannot prevent the gradual solvent degradation with cycling.

3.5. Stabilization of the SEI over calcium metal by using BF_3OEt_2

Bodin et al. showed that different BF_3 adducts employed as additives in various solvents appear to promote Ca plating [40]. The addition of 0.02 M $CaBF_3OEt_2$ to the 0.5 M $CaB_{12}H_{12}$@215/NMP electrolyte was therefore tested to improve the stability of the SEI layer on the calcium metal surface. The effect of this additive was evaluated by CV and compared to the performance of the pristine electrolyte, as illustrated in Fig. 8.

Even though both electrolytes show similar overpotentials, the addition of BF_3OEt_2 drastically improves the plating/stripping currents. These results suggest a remarkably beneficial impact of the additive on the electrokinetics of the calcium plating/stripping process at room temperature. As previously reported in the literature for other calcium-based electrolyte additives, one possible explanation is that the introduction of this additive weakens Ca^{2+}-anion interactions, thereby enhancing the Ca^{2+} desolvation kinetics. This effect could lead to more stable calcium plating and stripping processes [41,42]. The ESW of the 0.5 M $CaB_{12}H_{12}$@215/NMP electrolyte modified with 0.02 M BF_3OEt_2 is shown in Fig. S7.

Apparently, the use of BF_3OEt_2 reduces slightly the anodic stability of the electrolyte, limiting it at 2.75 V vs. Ca^{2+}/Ca. On the cathodic side, unlike the unmodified electrolyte (cf. Fig. 5a), an irreversible degradation is observed on the surface of the working electrode at 0.8–0.6 V vs. Ca^{2+}/Ca. This suggests a spontaneous degradation of the additive and the formation of redox-inactive by-products after the initial reduction.

The performance of the modified electrolyte in symmetric Ca | Electrolyte | Ca cells, evaluated by combined GC/EIS tests, is shown in Fig. 9.

The addition of BF_3OEt_2 to the electrolyte produces the following performance modifications:

(a) the magnitude of the galvanostatic overpotentials is only slightly modified compared to the pristine electrolyte (cf. Fig. 7a); a beneficial elimination of voltage spikes is observed at 0.01 and 0.1 mAh cm^{-2}, suggesting the possible suppression of gas release processes strongly affecting the electrochemically active surface of calcium electrodes (see Fig. 7a);
(b) the constant EIS spectra recorded during OCV before cycling indicate that the modified electrolyte is chemically inert on the calcium metal surface, similar to the unmodified electrolyte.
(c) the high frequency Z_{real} intercept in the EIS spectra increases upon cycling, thus suggesting the consumption of Ca^{2+} ions from the electrolyte solution, also similar to the unmodified electrolyte.

Overall, the impact of the BF_3OEt_2 additive has a partially positive effect on the stability of the Ca/electrolyte interface during cycling, resulting from a balance between the beneficial and the detrimental outcomes. A future perspective involves gaining insight into the morphology and evolution of the SEI by analysing its composition using surface characterization techniques, such as X-ray photoelectron spectroscopy.

4. Conclusion

This study demonstrates the use of a *closo* dodecaborate calcium salt, $CaB_{12}H_{12}$, synthesized by an easy route, to formulate aprotic electrolytes for calcium batteries: The major findings of this work include:

I. Calcium dodecaborate with few impurities can be synthesized at 215 °C, and dissolved in NMP up to a concentration of 0.5 M. The partial opalescence observed in the electrolytes is likely caused by synthesis by-products.
II. Electrolytes formulated in NMP exhibit limited ionic conductivity at room temperature and an ESW ranging from 0 to 3 V vs Ca^{2+}/Ca.
III. $CaB_{12}H_{12}$-based NMP electrolytes enable electrochemical plating of calcium metal on a gold substrate, as well as reversible plating/stripping of calcium metal under galvanostatic conditions.
IV. Parasitic reactions occur during cycling, although the electrolytes remain chemically inert in contact with calcium metal electrodes at room temperature.
V. The addition of BF_3OEt_2 as an electrolyte additive positively modifies the parasitic reactions and enhances the galvanostatic performance.

It is important to underline that the parasitic reactions involving the irreversible consumption of Ca^{2+} ions contained in the electrolytes may be promoted by residual synthesis impurities. Therefore, in order to improve the solubility of the salt, the optimisation of the synthesis to achieve a pure compound, and/or of the purification processes is a critical prerequisite for further research on this electrolyte salt, and for thoroughly assessing the potential of calcium dodecaborate-based electrolytes for calcium battery applications.

CRediT authorship contribution statement

Andrea Ceppetelli: Writing – original draft, Validation, Supervision, Methodology, Investigation, Formal analysis, Data curation, Conceptualization. **Carlos Castilla-Martinez:** Writing – review & editing, Supervision, Methodology, Investigation, Formal analysis, Data curation. **Eymerick Rousselot:** Investigation, Data curation. **Laure Monconduit:** Writing – review & editing, Supervision, Resources, Project administration, Methodology, Funding acquisition. **Umit B. Demirci:** Writing – review & editing, Validation, Supervision, Methodology, Investigation, Funding acquisition, Conceptualization. **Sergio Brutti:** Writing – review & editing, Writing – original draft, Validation, Supervision, Project administration, Methodology, Funding acquisition, Formal analysis, Conceptualization. **Lorenzo Stievano:** Writing – review & editing, Visualization, Validation, Supervision, Resources, Project administration, Methodology, Investigation, Funding acquisition, Conceptualization.

Declaration of competing interest

The authors declare the following financial interests/personal relationships which may be considered as potential competing interests: Lorenzo Stievano, Laure Monconduit reports financial support was provided by French National Research Agency. Lorenzo Stievano, Sergio Brutti reports financial support was provided by University of Oslo. Umit Demirci reports financial support was provided by University of Montpellier. Sergio Brutti reports financial support was provided by Centro nazionale per la mobilita sostenibile (MOST). If there are other authors, they declare that they have no known competing financial interests or personal relationships that could have appeared to influence the work reported in this paper.

Acknowledgments

The authors gratefully thank the Research Council of Norway for the financial support through the Calsiumbat project (project number 320670). This work was supported by the LabUM Chimie de the University of Montpellier and benefited from state aid managed by the National Agency for Research at title of the Future Investments program bearing the reference ANR-16-IDEX-0006. This research project was also supported by the “Centro Nazionale per la Mobilità Sostenibile (MOST) CN4 Spoke 13 Batterie e Transizione Elettrica” funded by the Italian Government and the European Union in the frame of the “Missione 4 Componente 2 Investimento 1.4 - Potenziamento strutture di ricerca e

creazione di “campioni nazionali di R&S00 su alcune Key Enabling Technologies del PNRR (Avviso MUR n. 3138 del 16-12-2021)”. Finally, ANR is gratefully acknowledged for funding through the project Labex STORE-EX (Grant ANR-10-LABX-76-01).

Appendix A. Supplementary data

Supplementary data to this article can be found online at https://doi.org/10.1016/j.est.2024.115012.

Data availability

Data will be made available on request.

References

[1] M.Y. Worku, Recent Advances in Energy Storage Systems for Renewable Source Grid Integration: A Comprehensive Review 14, 2022, p. 5985, https://doi.org/10.3390/su14105985.
[2] C. Wang, X. Wang, R. Zhang, T. Lei, K. Kisslinger, H.L. Xin, Resolving complex intralayer transition motifs in high-Ni-content layered cathode materials for lithium-ion batteries, Nat. Mater. 22 (2) (2023) 235–241, https://doi.org/10.1038/s41563-022-01461-5 ((2023 22:2).
[3] K. Xu, Electrolytes and interphases in Li-ion batteries and beyond, Chem. Rev. 114 (23) (2014) 11503–11618, https://doi.org/10.1021/CR500003W.
[4] E.C. Evarts, Lithium batteries: to the limits of lithium, Nature 526 (7575) (2015) S93–S95, https://doi.org/10.1038/526s93a (2015 526:7575).
[5] K. Xu, Nonaqueous liquid electrolytes for lithium-based rechargeable batteries, Chem. Rev. 104 (10) (2004) 4303–4417, https://doi.org/10.1021/CR030203G/ASSET/IMAGES/LARGE/CR030203GF00018.JPEG.
[6] European Commission. European Comission, Critical Raw Materials Resielience: Charting a Path towards Greater Security and Sustainability, Communication COM (2020) 474, Https://Eur-Lex.Europa.Eu/Legal-Content/EN/TXT/HTML/?Uri=CELEX:52020DC0474&from=EN (Final, 20.4.2022). 2020.
[7] R.J. Gummow, G. Vamvounis, M.B. Kannan, Y. He, Calcium-ion batteries: current state-of-the-art and future perspectives, Adv. Mater. 30 (39) (2018) 1801702, https://doi.org/10.1002/adma.201801702.
[8] M.E. Arroyo-De-Dompablo, A. Ponrouch, P. Johansson, M.R. Palacín, M.E. Arroyo-De Dompablo, A. Ponrouch, P. Johansson, M.R. Palacín, Achievements, challenges, and prospects of calcium batteries, Chem. Rev. 120 (14) (2019) 6331–6357, https://doi.org/10.1021/acs.chemrev.9b00339.
[9] L. Stievano, I. de Meatza, J. Bitenc, C. Cavallo, S. Brutti, M.A. Navarra, Emerging calcium batteries, J. Power Sources 2021 (482) (August 2020) 228875, https://doi.org/10.1016/j.jpowsour.2020.228875.
[10] A. Ponrouch, C. Frontera, F. Bardé, M.R. Palacín, Towards a calcium-based rechargeable battery, Nat. Mater. 15 (2) (2015) 169–172, https://doi.org/10.1038/nmat4462 (2015 15:2).
[11] M. Kotobuki, B. Yan, L. Lu, Recent progress on cathode materials for rechargeable magnesium batteries, Energy Storage Mater. 2023 (54) (October 2022) 227–253, https://doi.org/10.1016/j.ensm.2022.10.034.
[12] Z. Hou, R. Zhou, Y. Yao, Z. Min, Z. Lu, Y. Zhu, J.M. Tarascon, B. Zhang, Correlation between electrolyte chemistry and solid electrolyte interphase for reversible ca metal anodes, Angew. Chem. Int. Ed. 61 (50) (2022) e202214796, https://doi.org/10.1002/ANIE.202214796.
[13] D. Wang, X. Gao, Y. Chen, L. Jin, C. Kuss, P.G. Bruce, Plating and stripping calcium in an organic electrolyte, Nat. Mater. 17 (1) (2017) 16–20, https://doi.org/10.1038/nmat5036 (2017 17:1).
[14] Z. Li, O. Fuhr, M. Fichtner, Z. Zhao-Karger, Towards stable and efficient electrolytes for room-temperature rechargeable calcium batteries, Energy Environ. Sci. 12 (12) (2019) 3496–3501, https://doi.org/10.1039/C9EE01699F.
[15] T. Pavčnik, J.D. Forero-Saboya, A. Ponrouch, A. Robba, R. Dominko, J. Bitenc, A novel calcium fluorinated alkoxyaluminate salt as a next step towards ca metal anode rechargeable batteries, J. Mater. Chem. A 11 (27) (2023) 14738–14747, https://doi.org/10.1039/d3ta02084c.
[16] J. Luo, Y. Bi, L. Zhang, X. Zhang, T.L. Liu, A stable, non-corrosive perfluorinated pinacolatoborate Mg electrolyte for rechargeable Mg batteries, Angew. Chem. Int. Ed. 58 (21) (2019) 6967–6971, https://doi.org/10.1002/anie.201902009.
[17] K. Kisu, S. Kim, T. Shinohara, K. Zhao, A. Züttel, S. ichi Orimo, Monocarborane cluster as a stable fluorine-free calcium battery electrolyte, Sci. Rep. *11* (1) (2021) 1–8, https://doi.org/10.1038/s41598-021-86938-0 *(2021 11:1)*.
[18] *Cesium (CAS Number 12539-26-3) : Strem Product Catalog*. https://www.strem.com/catalog/v/55-5525/cesium_12539-26-3 (accessed 2023-11-09).
[19] J. Wang, T. Steenhaut, H.-W. Li, Y. Filinchuk, High yield autoclave synthesis of pure M 2 B 12 H 12 (M = Na, K), Inorg. Chem. 62 (2023), https://doi.org/10.1021/acs.inorgchem.2c03810.
[20] Grahame, A.; Aguey-Zinsou, K.-F. Inorganics Properties and Applications of Metal (M) Dodecahydro-Closo-Dodecaborates (M N=1,2 B 12 H 12) and Their Implications for Reversible Hydrogen Storage in the Borohydrides. doi:https://doi.org/10.3390/inorganics6040106.
[21] First-Principles Study of CaB 12 H 12 as a Potential Solid-State Conductor for Ca. 2020. doi:10.1039/x0xx00000x.
[22] Gigante, A.; Løod; Moury, R.; Pupier, M.; Remhof, A.; Hagemann, H. Direct Solution-based Synthesis of Na 4 (B 12 H 12)(B 10 H 10)S Olid Electrolyte. doi:https://doi.org/10.1002/cssc.201902152.
[23] J. Wang, T. Steenhaut, H.-W. Li, Y. Filinchuk, High yield autoclave synthesis of pure M2B12H12 (M = Na, K), Inorg. Chem. (2023), https://doi.org/10.1021/ACS.INORGCHEM.2C03810.
[24] R. Moury, A. Gigante, H. Hagemann, An alternative approach to the synthesis of NaB3H8 and Na2B12H12 for solid electrolyte applications, Int. J. Hydrog. Energy 42 (35) (2017) 22417–22421, https://doi.org/10.1016/J.IJHYDENE.2017.02.044.
[25] S. Pylypko, S. Ould-Amara, A. Zadick, E. Petit, M. Chatenet, M. Cretin, U. B. Demirci, The highly stable aqueous solution of sodium dodecahydro-closo-dodecaborate Na2B12H12 as a potential liquid anodic fuel, Appl Catal B 222 (2018) 1–8, https://doi.org/10.1016/J.APCATB.2017.09.068.
[26] S. Ould-Amara, E. Petit, D. Granier, P.G. Yot, U.B. Demirci, Alkaline aqueous solution of sodium decahydro-closo-decaborate Na2B10H10 as liquid anodic fuel, Renew. Energy 143 (2019) 551–557, https://doi.org/10.1016/J.RENENE.2019.05.019.
[27] A. Liu, S. Xie, S. Dabiran-Zohoory, Y. Song, High-pressure Structures and Transformations of Calcium Borohydride Probed by Combined Raman and Infrared Spectroscopies, 2010, https://doi.org/10.1021/jp1009115.
[28] E.M. Dematteis, M. Baricco, Hydrogen desorption in Mg(BH4)2-Ca(BH4)2 system, Energies 12 (17) (2019) 3230, https://doi.org/10.3390/EN12173230 (2019, Vol. 12, Page 3230).
[29] Y. Sadikin, E. Didelot, Z. Łodziana, R. Černý, Synthesis and crystal structure of solvent-free dodecahydro closo-dodecaborate of nickel, NiB12H12, Dalton Trans. 47 (16) (2018) 5843–5849, https://doi.org/10.1039/C8DT00381E.
[30] I.K. Kochneva, V.V. Avdeeva, I.N. Polyakova, E.A. Malinina, Mixed-ligand polymeric and binuclear silver(I) complexes with the dodecahydro-closo-dodecaborate anion and bipyridylamine, Polyhedron 109 (2016) 19–25, https://doi.org/10.1016/J.POLY.2016.01.045.
[31] E. Didelot, Y. Sadikin, Z. Łodziana, R. Černý, Hydrated and anhydrous dodecahydro closo-dodecaborates of 3d transition metals and of magnesium, Solid State Sci. 90 (2019) 86–94, https://doi.org/10.1016/J.SOLIDSTATESCIENCES.2019.02.005.
[32] *Product E001 / 1M LiPF6 in EC:DMC (1:1 vol.%) 99.9%*. https://en.solvionic.com/products/1m-lipf6-in-ec-dmc-1-1-vol.-99.9 (accessed 2023-10-04).
[33] J.D. Forero-Saboya, E. Marchante, R.B. Araujo, D. Monti, P. Johansson, A. Ponrouch, Cation solvation and physicochemical properties of Ca battery electrolytes, J. Phys. Chem. C 123 (49) (2019) 29524–29532, https://doi.org/10.1021/ACS.JPCC.9B07308/ASSET/IMAGES/LARGE/JP9B07308_0005.JPEG.
[34] C. Zhou, J.B. Grinderslev, L.N. Skov, M. Jørgensen, Y. Li, J. Skibsted, Y. Yan, T. R. Jensen, Polymorphism, ionic conductivity and electrochemical properties of lithium closo-deca- and dodeca-borates and their composites, Li2B10H10–Li2B12H12, J. Mater. Chem. A Mater. 10 (30) (2022) 16137–16151, https://doi.org/10.1039/D2TA00337F.
[35] B. Ng, P.T. Coman, E. Faegh, X. Peng, S.G. Karakalos, X. Jin, W.E. Mustain, R. E. White, Low-temperature lithium plating/corrosion hazard in lithium-ion batteries: electrode rippling, variable states of charge, and thermal and nonthermal runaway, ACS Appl. Energy Mater. 3 (4) (2020) 3653–3664, https://doi.org/10.1021/ACSAEM.0C00130.
[36] S. Sarkar, V. Thangadurai, Critical current densities for high-performance all-solid-state Li-metal batteries: fundamentals, mechanisms, interfaces, materials, and applications, ACS Energy Lett. 7 (4) (2022) 1492–1527, https://doi.org/10.1021/ACSENERGYLETT.2C00003/ASSET/IMAGES/LARGE/NZ2C00003_0021.JPEG.
[37] J. Yang, C. Hu, H. Wang, K. Yang, J.B. Liu, H. Yan, Review on the research of failure modes and mechanism for lead–acid batteries, Int. J. Energy Res. 41 (3) (2017) 336–352, https://doi.org/10.1002/ER.3613.
[38] S. Wang, P. Takyi-Aninakwa, S. Jin, C. Yu, C. Fernandez, D.I. Stroe, An improved feedforward-long short-term memory modeling method for the whole-life-cycle state of charge prediction of lithium-ion batteries considering current-voltage-temperature variation, Energy 254 (2022) 124224, https://doi.org/10.1016/J.ENERGY.2022.124224.
[39] S.D. Talian, S. Brutti, M.A. Navarra, J. Moškon, M. Gaberscek, Impedance spectroscopy applied to lithium battery materials: good practices in measurements and analyses, Energy Storage Mater 69 (2024) 103413, https://doi.org/10.1016/J.ENSM.2024.103413.
[40] C. Bodin, J. Forero Saboya, P. Jankowski, K. Radan, D. Foix, C. Courrèges, I. Yousef, R. Dedryvère, C. Davoisne, M. Lozinšek, A. Ponrouch, Boron-based functional additives enable solid electrolyte interphase engineering in calcium metal battery, Batter Supercaps 6 (1) (2023) e202200433, https://doi.org/10.1002/BATT.202200433.
[41] H. Song, Y. Li, F. Tian, C. Wang, Electrolyte optimization and interphase regulation for significantly enhanced storage capability in Ca-metal batteries, Adv. Funct. Mater. 32 (21) (2022), https://doi.org/10.1002/ADFM.202200004.
[42] H. Song, C. Wang, Current status and challenges of calcium metal batteries, Adv. Energy Sustain. Res. 3 (3) (2022) 2100192, https://doi.org/10.1002/AESR.202100192.